Analyst

PAPER

View Article Online
View Journal | View Issue

Cite this: *Analyst*, 2016, **141**, 2887

Real-time monitoring of calcification process by *Sporosarcina pasteurii* biofilm†

Dustin Harris,‡[a] Jyothir Ganesh Ummadi,‡[a] Andrew R. Thurber,[b] Yvan Allau,[b] Circe Verba,[c] Frederick Colwell,[b] Marta E. Torres[b] and Dipankar Koley*[a]

Sporosarcina pasteurii is known to produce calcite or biocement in the presence of urea and Ca^{2+}. Herein, we report the use of novel ultramicrosensors such as pH, Ca^{2+}, and redox sensors, along with a scanning electrochemical microscope (SECM), to monitor a real-time, bacteria-mediated urea hydrolysis process and subsequent changes in morphology due to $CaCO_3$ precipitation. We report that the surface pH of a live biofilm changed rapidly from 7.4 to 9.2 within 2 min, whereas similar fast depletion (10 min) of Ca^{2+} was observed from 85 mM to 10 mM in the presence of a high urea (10 g L^{-1}) brine solution at 23 °C. Both the pH and the Ca^{2+} concentration profiles were extended up to 600 μm from the biofilm surface, whereas the bulk chemical composition of the brine solution remained constant over the entire 4 h of SECM experiments. In addition, we observed a change in biofilm surface morphology and an increase in overall biofilm height of 50 μm after 4 h of precipitation. Electron microscopy confirmed the changes in surface morphology and formation of $CaCO_3$ crystals. Development of the Ca^{2+} profile took 10 min, whereas that of the pH profile took 2 min. This finding indicates that the initial urea hydrolysis process is fast and limited by urease or number of bacteria, whereas later $CaCO_3$ formation and growth of crystals is a slow chemical process. The ultramicrosensors and approaches employed here are capable of accurately characterizing bioremediation on temporal and spatial scales pertinent to the microbial communities and the processes they mediate.

Received 3rd January 2016,
Accepted 27th February 2016

DOI: 10.1039/c6an00007j

www.rsc.org/analyst

Introduction

Microbial-mediated carbonate precipitation has been widely used in building restoration, bioremediation of divalent ions (Pb^{2+}, Zn^{2+}) in contaminated aquifers, and control of atmospheric CO_2 by geologic carbon sequestering, especially in unmined coal seams and oil reserves.[1–4] However, the major problem in carbon sequestrating strategies is the leakage of low-density liquid CO_2 through porous rock structure. To prevent leakage in such a remote environment, one of the best option is to block the porous structure with calcium carbonate ($CaCO_3$), in particular by using bacterially mediated $CaCO_3$ precipitation, as such reactions can easily occur in dark and remote places.[5,6] Several ureolytic bacteria, such as *Sporosarcina pasteurii* (formerly known as *Bacillus pasteurii*), have been explored for microbial-mediated $CaCO_3$ precipitation. The microbial urease enzyme hydrolyzes the urea and produces dissolved ammonium ions, which increase the local pH and ultimately cause precipitation of $CaCO_3$ in the presence of a solution rich in calcium ions.[7–11] The negatively charged bacterial surface acts as a nucleation point to initiate this precipitation until the bacteria are encapsulated with thick $CaCO_3$ layers.[12] The reactions occur in the following sequence:

$$CO(NH_2)_2 + 2H_2O \rightarrow H_2CO_3 + 2NH_3$$

$$2NH_3 + 2H_2O \leftrightarrow 2NH_4^+ + 2OH^-$$

$$H_2CO_3 \leftrightarrow H^+ + HCO_3^-$$

$$HCO_3^- + H^+ + 2OH^- \leftrightarrow CO_3^{2-} + 2H_2O$$

$$CO_3^{2-} + Ca^{2+} \leftrightarrow CaCO_3$$

Overall reaction:

$$CO(NH_2)_2 + 2H_2O + Ca^{2+} \leftrightarrow 2NH_4^+ + CaCO_3$$

Several factors are known to affect this complex process, such as pH, amount of bacterial enzymes, temperature,

[a]*Department of Chemistry, Oregon State University, Corvallis, OR 97331, USA. E-mail: Dipankar.Koley@oregonstate.edu*
[b]*College of Earth, Ocean and Atmospheric Sciences, Oregon State University, Corvallis, OR 97331, USA*
[c]*Department of Energy, National Energy Technology Laboratory, 1450 Queen Ave SE, Albany, OR 97322, USA*
†Electronic supplementary information (ESI) available. See DOI: 10.1039/c6an00007j
‡These authors contributed equally to this work.

concentration of calcium ions, presence of nucleation sites, and ionic strength.[13] Bacteria with high zeta potential have shown higher adhesion efficiency and thus an enhanced rate of carbonate precipitation.[14,15] The enzyme-mediated urea hydrolysis reaction depends on temperature; as in other enzymatic reactions, the rate of ureolysis increases with increasing temperature. Ferris *et al.*[16,17] reported that the rate of ureolysis increases by 5 times with an increase in temperature from 15 to 20 °C. Increasing the ionic strength from 0.1 to 1.0 increases the equilibrium constant for ammonium speciation from 9.3 to 9.4, as the higher ionic strength tends to increase the electrical double layer (EDL) compression and thus decreases the EDL repulsive force, leaving the van der Waals attractive force as the predominant force and ultimately promoting carbonate-mediated bacteria adhesion.[18,19]

While we have a basic understanding of those factors that influence the precipitation of $CaCO_3$ as a result of urea hydrolysis, we lack quantitative chemical data on a scale appropriate to characterizing this reaction. Studies focused on the kinetic and chemical reactions involved in this the ureolytic process are taken from bulk fluid measurments,[20–23] however the reaction occurs on the surface or adjacent to the surface of bacteria, meaning that the bulk measurements do not represent the mechanism involved. This lacking quantitative chemical data (pH, Ca^{2+}, and NH_4^+ concentrations; thickness of $CaCO_3$ precipitation) at an appropriate high spatial and temporal resolution limits the potential application and resulting accuracy of mathematical models of the process. This is further challenged by the extremely complex combination of physical, chemical, and biological processes occurring in microbial-mediated carbonate precipitation.[24–26] Thus the following important questions remain unanswered: How do the bacteria in biofilm communities interact with the local physical and chemical environments? How fast does the local pH and Ca^{2+} concentration change above the biofilm? What morphological changes occur in real time as $CaCO_3$ precipitates on live biofilm?

The main challenge in answering these questions is the lack of an analytical technique to measure the chemical parameters in high spatial and temporal resolution. One of the best alternative analytical techniques is the scanning electrochemical microscope (SECM). In this technique, the scanning probe (25 μm diameter or less) can be positioned precisely in the micrometer range with the aid of a probe approach curve method.[27] The SECM has been widely used in biological systems, including microbial biofilms.[28–32] Several studies of pH mapping have been reported that used polyaniline, Sb/SbO_2, or Ir/IrOx to map yeast metabolites; the surface pH of endothelial cells; and rat kidney surfaces.[33–36] Etienne *et al.*[37] reported a similar SECM study in which they used a Ca^{2+} sensor as an SECM probe to study the dissolution of calcite crystals. However, they did not report any quantitative Ca^{2+} distribution data.

In the present study, we used a new electrochemical technique, scanning electrochemical microscopy, to quantify the local chemical change by using live *S. pasteurii* biofilm. Brine solution was used in this study to replicate the high ionic strength and Ca^{2+}-rich solution that is relevant in oil well applications and the Mount Simon carbon sequestering program.[38–40] We use a novel proton ion-selective microelectrode (H^+-ISME) and a Ca^{2+}-selective microelectrode (Ca^{2+}-ISME) to quantify the local pH and Ca^{2+} gradients, respectively. The fundamental data obtained in this study might be useful in future mathematical modeling and thus improve the design of *S. pasteurii*-based $CaCO_3$ applications besides answering some of the basic questions such as the interactions of biofilm with the immediate environment and the real-time morphological changes of biofilm due to $CaCO_3$ precipitation, *etc.*

Materials and methods

Chemicals

ETH 129 (Ca^{2+} ionophore) and high molecular weight Poly(vinyl chloride) (PVC) and yeast extract were purchased from Sigma Aldrich. 1-Nitro-2-(*n*-octyloxy)benzene (NPOE) was purchased from Alfa Aesar. Bis(2-ethylhexyl)sebacate (DOS) and potassium tetrakis(4-chlorophenyl)borate (KTPIB) were purchased from TCI America. Aniline (99%), HCl, $CaCl_2$, urea, and $(NH_4)_2SO_4$ were purchased from Macron Fine Chemicals. NaCl, potassium ferrocyanide ($K_4[Fe(CN)_6]$), $MgCl_2$, Na_2SO_4, and $NaHCO_3$ and Tetrahydrofuran (THF) were purchased from EMD Chemicals. TRIS Base was purchased from JT Baker, agar from Spectrum. All chemicals were used as purchased without further purifications. Vulcan carbon powder was a kind gift from Cabot Corporation. The brine composition used in all experiments was as follows: 1.02 M NaCl, 0.17 M $CaCl_2$, 0.06 M $MgCl_2$ 0.02 M Na_2SO_4, and 0.01 M $NaHCO_3$ representative of the Mt. Simon formation (Illinois State Geological Survey). All solutions were prepared with 18 MΩ DI water (Elga Water Systems).

Instrumentation

All electrochemical measurements were performed by using a scanning electrochemical microscope (SECM) (CHI 920D). A separate high impedance unit (EA Instruments) was used with SECM to perform potentiometric experiments. Ag/AgCl and a 0.5 mm Pt wire were used as reference and counter electrodes, respectively.

Fabrication of pH microsensor

A theta pipet (1.5 mm o.d./1 mm i.d.) was first pulled by using a gravity pipette puller. A 25 μm diameter Pt wire (Goodfellow Cambridge Ltd) was inserted into each channel of the pulled theta pipette and the end was sealed vertically with a heating coil under vacuum. Each cavity of the sealed pipette was then backfilled with silver epoxy and copper wires for electrical connection. The potentiometric pH sensor was made by electrochemically depositing polyaniline onto one of the two bare Pt electrode surfaces. The polyaniline was deposited by cycling potential between −0.2 V and +1.0 V (*vs.* Ag/AgCl) for 50 cycles at 0.1 V s^{-1} in 0.1 M aniline and 1 M HCl. The dual SECM

probe was used as follows: *Electrode* 1: bare Pt electrode to perform amperometric approach curve; *Electrode* 2: Pt/polyaniline electrode or pH microsensor was calibrated in brine by adding aliquots of 1 M HCl and 1 M NaOH prior to SECM experiments.

Fabrication of Ca^{2+} selective microelectrode (Ca^{2+}-ISME)

The Ca^{2+}-sensing carbon paste was prepared by combining (w/w): 5% ETH 129, 3% PVC, 2% KTIPB, 30% NPOE, and 60% carbon powder. This paste was packed inside a 25–35 μm diameter pulled borosilicate pipette (1.5 mm o.d./0.86 mm i.d.). A separate carbon paste (2.6 (w/w%) of Vulcan carbon in DOS) was used as a back contact with copper wire and sensing membrane paste (Fig. 1). The Ca^{2+}-ISME electrode was then cured in 10 mM $CaCl_2$ solution for at least 12 h before use. The sensor was calibrated in brine solution by the standard addition method. For SECM experiments, the Ca^{2+}-ISME was used to perform amperometric approach curve in presence of 1 mM ferrocyanide containing brine solution. Later the solution was replaced by brine solution to measure [Ca^{2+}] profile produced by biofilm using the same Ca^{2+}-ISME by potentiometric method.

Preparation of membrane biofilm

S. pasteurii was purchased from the American Type Culture Collection (ATCC; strain 11859) and was maintained in ATCC growth medium 1376. The composition of the ATCC growth medium was as follows: 0.13 M Tris buffer (pH 9), 10.0 g L^{-1} $(NH_4)_2SO_4$, 20.0 g L^{-1} yeast extract, and 20.0 g L^{-1} agar (for gel plates). A 5 mL aerobic culture tube containing 3 mL of media was inoculated with *S. pasteurii*, having an initial optical density (OD_{600}) of 0.025. After 2 days of incubation at 30 °C, bacteria from logarithmic growth phase were used to prepare biofilm samples. A 1 mL aliquot of liquid culture was centrifuged and washed in brine two times to prevent calcium phosphate precipitation in the presence of brine. After washing, the bacteria were resuspended in brine with an OD_{600} of 0.1. Suspended bacteria (2.5 μL) were then pipetted and plated over a sterile 0.2 μm diameter pore size polycarbonate membrane, which was placed over a nutrient containing agar plate (see Fig. S1A†). The bacteria-containing membrane/agar plate was later incubated at 30 °C for 72 h. The biofilms prepared in this method allowed us to obtain reproducible samples (2 mm diameter) of uniform bacterial number and percent coverage, as they are physically constrained on the membrane due to an absence of any liquid media. Before each SECM experiment, the membrane-biofilm was removed carefully from the agar plate using forceps and was affixed at the bottom of a small petri dish with double-sided tape and subsequently placed on the SECM stage. The biofilm was then exposed to brine (5 mL) with 1 g L^{-1} urea for 1 min in the petri dish to prevent the flotation of biofilm in solution, thus making it suitable for further SECM experiments.

SECM experiments for pH and Ca^{2+} profile above the biofilms

The dual-SECM pH probe, *i.e.*, one a Pt electrode and the other a pH sensing electrode, was used for all biofilm pH profile experiments (Fig. 1). At first, the probe-biofilm distance was

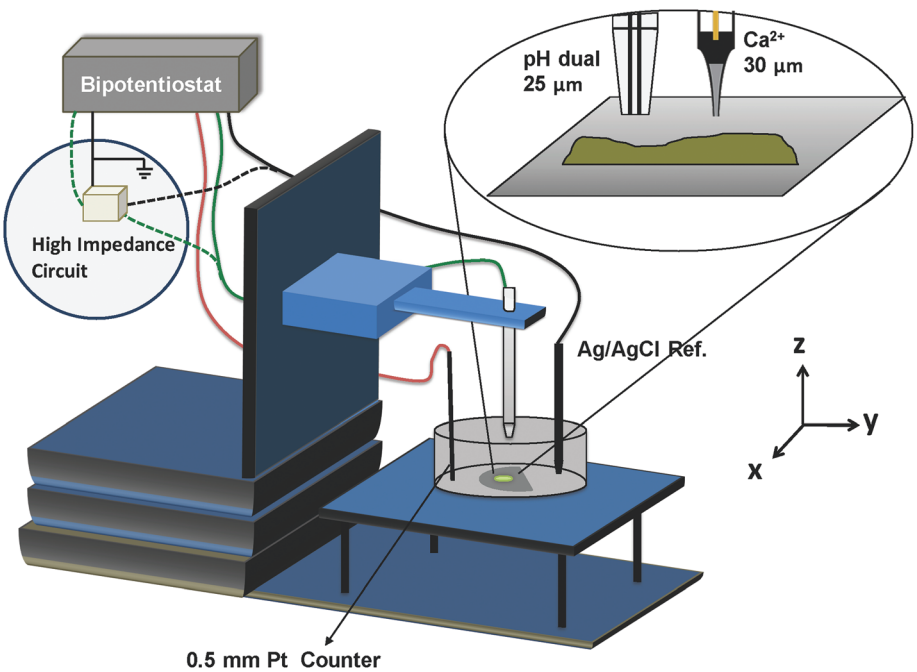

Fig. 1 Schematic diagram of the SECM biofilm experimental setup. Shown in the inset are the dual-electrode pH sensor with Pt and Pt/polyaniline (left) and the dual-function Ca^{2+} sensor (right). In the pH sensor, the bare Pt electrode was used for performing approach curve while the Pt/polyaniline electrode function as a pH sensor. The Ca^{2+} sensing SECM probe was used both for performing approach curve and also for potentiometric Ca^{2+} measurements.

determined by performing a negative feedback amperometric approach curve using the bare Pt electrode in a 2 mM ferrocyanide and brine solution. The exact location of approach curve, regarding absolute x and y-position, was then noted, and subsequent experiments were performed at the same location to avoid any discrepancies for such a rough surface biofilm sample. The solution was then replaced by a brine solution containing 1 g L^{-1} or 10 g L^{-1} urea and the pH sensor was turned on to record the potential with respect to time. The potential was recorded by using the high impedance unit. Later, the pH gradient above the biofilm (in the z-direction) was mapped by moving the pH probe in the z-direction at the speed of 1 μm s^{-1}. All SECM experiments were performed at 23 °C. The pH probe was calibrated after each SECM experiment and the calibration curve was used to convert the potential to pH value.

Measurements of Ca^{2+} exactly followed this method with the exception that the same Ca^{2+}-ISME of 25 μm diameter probe was used for performing amperometric approach curve as well as potentiometrically measuring the Ca^{2+} profiles above the live biofilm (please see fabrication of Ca^{2+}-ISME section above).

Height and morphology of $CaCO_3$ precipitation on biofilm

A single 25 μm diameter Pt electrode was used to determine $CaCO_3$ precipitation and subsequent morphological changes over the live biofilm. A series of approach curves at six different locations on the biofilm were performed to determine the change in biofilm height due to $CaCO_3$ precipitation. The urea-containing brine solution was temporarily replaced by a brine solution and 2 mM ferrocyanide to perform these negative approach curves.

SECM images of the biofilm surface topography were performed on biofilm after 15 min and 4 h of exposure to 10 g L^{-1} urea in brine at 23 °C. The tip was positioned approximately 10 μm away from the highest observed topographical feature. The tip was then scanned at a constant height in a 500 × 500 μm window.

Scanning electron microscopy (SEM) analysis of biofilms

S. pasteurii biofilms prepared as described above were imaged by SEM after immersed in brine and urea (1 g L^{-1} and 10 g L^{-1}) for 0.25, 4, 24, and 96 h. The biofilms were stored at −20 °C until SEM microanalysis were performed. Fixative (50 μL) (2.5% glutaraldehyde, 1% paraformaldehyde in 0.1 M sodium cacodylate buffer) was applied to the biofilms for 4 h at room temperature. The biofilm was rinsed in sodium cacodylate buffer. Samples were then dehydrated with increasing concentrations of acetone (10%, 30%, 50%, 70%, 90%, 100%) for 15 min and allowed to evaporate in fumehood. Samples were fixed to aluminum stubs with copper tape and sputter coated with gold/palladium (60/40). An FEI Quanta 600 Field Emission Gun SEM with a lithium-drifted silicon solid-state energy dispersive X-ray detector at 8 kV with a spot size of 5 was used to acquire backscattered electron images and characteristic X-ray spectra.

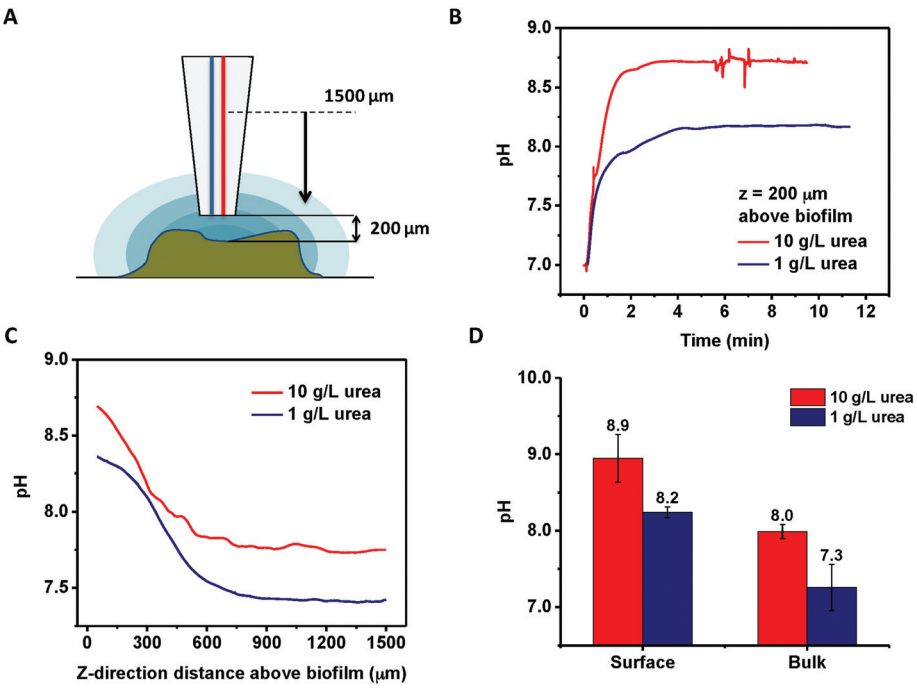

Fig. 2 (A) Schematic diagram of pH mapping above the biofilm using SECM. (B) A representative data showing change in local pH at 200 μm above the biofilm at 23 °C. (C) Representative z-direction pH scans from 20 to 1500 μm above the biofilm during exposure to brine solution containing 1 and 10 g L^{-1} urea at 23 °C. (D) Average surface pH in the presence of 1 g L^{-1} or 10 g L^{-1} urea as measured by SECM. Data were normalized according to bulk pH measurements.

Results and discussion

Characterization of pH and Ca^{2+}-ISME

The pH microsensor was calibrated in brine solution by adding aliquots of 1.0 M HCl and 1.0 M NaOH at 23 °C. pH sensors with a slope of 59 ± 10 mV pH^{-1} and a linear dynamic range of 6.0–9.5 were used for further SECM experiments. Fig. S1B† shows a representative calibration curve of the pH sensor in brine and urea (both 1 g L^{-1} and 10 g L^{-1} urea). However, we restricted our pH measurements to within 2–3 h,

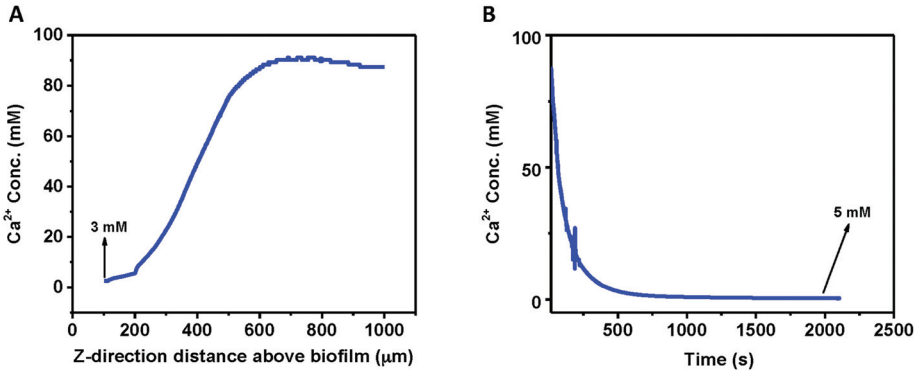

Fig. 3 (A) Representative *z*-scan of the Ca^{2+} profile above the biofilm in the presence of brine and 10 g L^{-1} urea. The profile extends to approximately 600 μm above the biofilm surface. (B) Development of a local decrease in Ca^{2+} concentration due to calcification over a half-hour period in the presence of 10 g L^{-1} urea in brine. The sensor was held at 200 μm above the biofilm during the measurement.

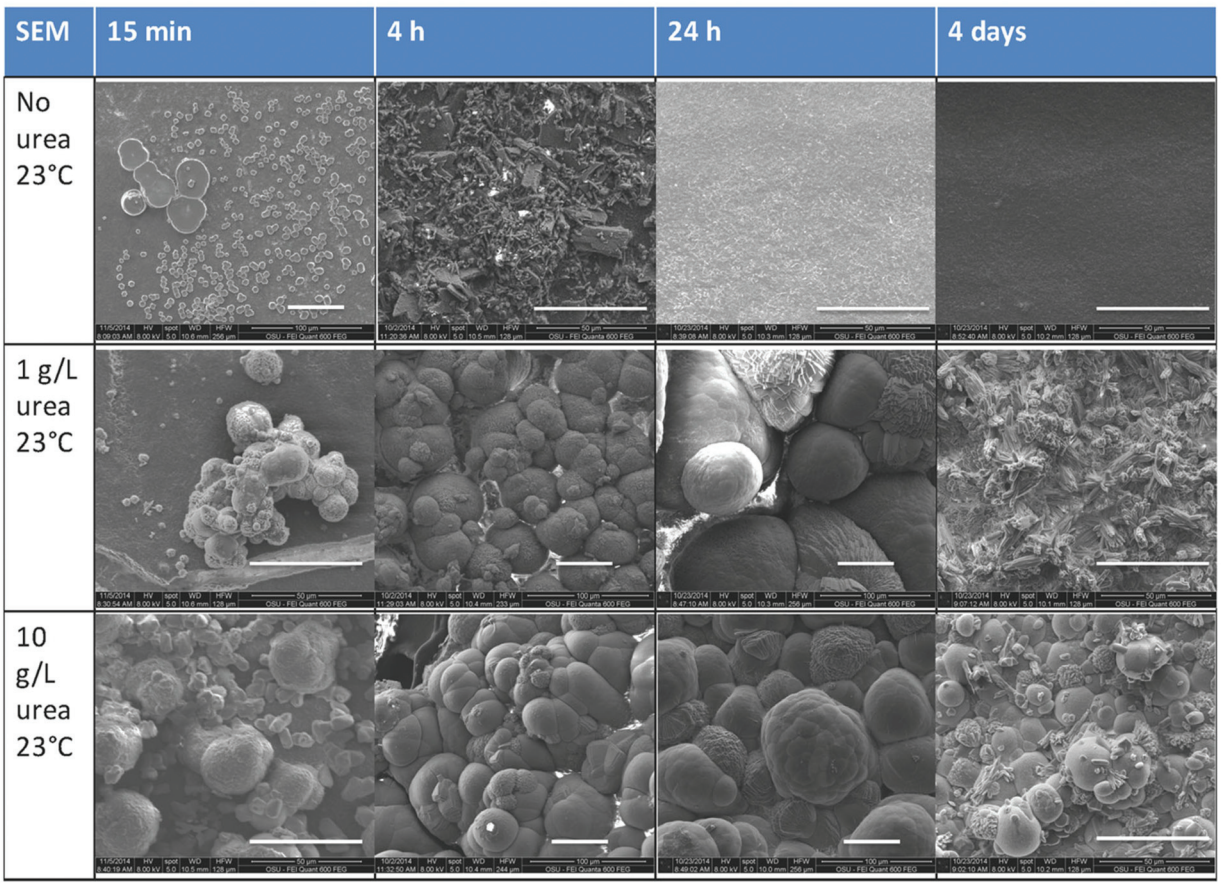

Fig. 4 Scanning electron micrograph (SEM) images of biofilms exposed to brine solution without urea, with a low urea concentration (1 g L^{-1}), and with a high urea concentration (10 g L^{-1}) at 23 °C. Scale bar: 50 μm.

as the sensor started to lose its stability as a result of exposure to the high ionic strength brine solution.

The Ca^{2+}-ISME was calibrated in brine solution (pH of 4.5) at 23 °C. The sensor had a linear response in the range of 100 μM – 200 mM with a slope of 26 ± 2 mV per log [Ca^{2+}] (Fig. S2A†) and showed a response time of 0.5 s (Fig. S2B†). The stability of the sensor was 2 mV drift in 2 h, which was the maximum time for the experiment.

Real-time quantification of pH gradient above *S. pasteurii* biofilm

S. pasteurii biofilms hydrolyze the urea present in the brine solution and cause the local pH to rise, which ultimately causes the $CaCO_3$ to precipitate (Fig. 2A). Thus, it is essential to quantify the local pH, as this is an indication of the rate of hydrolysis. Fig. 2B shows the rise of local pH at a distance of 200 μm above the biofilm in the presence of brine containing 1 g L^{-1} and 10 g L^{-1} urea. As expected, the local pH increased from the initial value of 7.0 to a steady-state value in 1.5 ± 0.5 min in the presence of 10 g L^{-1} urea and in 6.2 ± 2 min in the presence of 1 g L^{-1} urea. The surface pH gradient above the biofilm formed more quickly in the presence of 10 g L^{-1} urea, and the surface pH was higher than in the presence of 1 g L^{-1} urea. The steady-state local pH was estimated to be 8.7 ± 0.5 and 8.4 ± 0.5 for 10 g L^{-1} and 1 g L^{-1} urea, respectively (Fig. 2B).

To estimate how far the pH was extended, we performed a *z*-direction pH scan from 20 μm to 1500 μm above the biofilm surface. Fig. 2C is a representative *Z*-scan in which the pH gradient extended up to 600 μm above the biofilm. The average surface pH was 8.9 compared with a bulk pH of 8.0 after 30 min of exposure to brine and 10 g L^{-1} urea, whereas the surface pH was 8.0 relative to a bulk pH of 7.3 in the case of 1 g L^{-1} urea (Fig. 2D and Fig. S3†).

Real-time quantification of Ca^{2+} gradient above the biofilm

To measure the "depletion layer" of Ca^{2+} at the biofilm surface we performed analogous chemical profile experiments with the Ca^{2+}-ISME, including Ca^{2+} profile development and quasi-steady-state profile *z*-scans. The Ca^{2+} *z*-scan profile shows a significantly decreased Ca^{2+} concentration near the surface of the biofilm, from 85 mM in the bulk (1000 μm) solution to 1–6 mM near the surface (Fig. 3A). This profile developed on the same timescale as the development of the pH profile (6–10 min), which follows from the mechanism of bacteria-induced precipitation (Fig. 3B). The Ca^{2+} profile extends to 600 μm above the surface, which is the same extent as the pH profile. This shows that the pH profile causes $CaCO_3$ precipitation, which then drives the flux of Ca^{2+} ions to the surface,

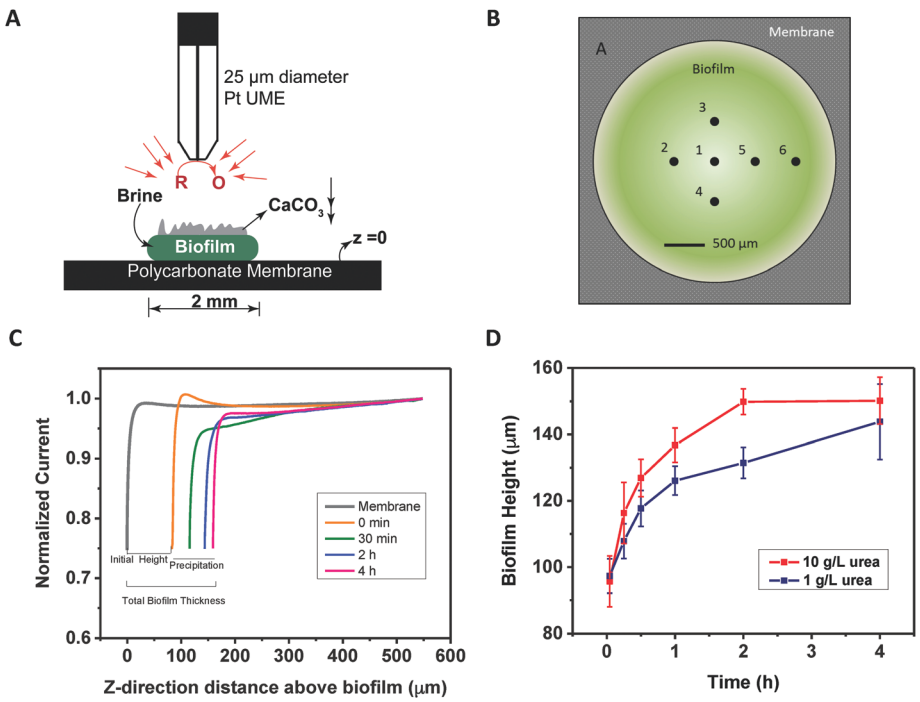

Fig. 5 (A) Schematic diagram of an SECM probe showing how the blocking of redox molecules gives rise to topographical data about a biofilm mediated calcification process. R and O represent reduced and oxidized species respectively. (B) Biofilm plated on a membrane was exposed to brine with urea and the height of the biofilm was measured at multiple points. (C) The membrane surface is considered as the reference point (z = 0) to calculate the initial biofilm height. A series of representative approach curves on a given point at the center of the biofilm. The figure shows the initial biofilm height and the increase in height because of $CaCO_3$ precipitation. (D) Change in average biofilm height due to $CaCO_3$ precipitation over 4 h. The red line and squares indicate the measured height after exposure to 10 g L^{-1} urea, and the blue line and squares indicate the increase in height after exposure to 1 g L^{-1} urea.

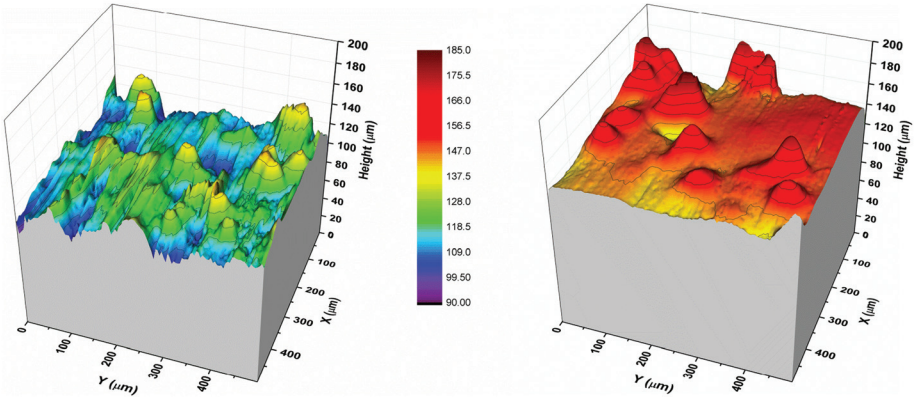

Fig. 6 SECM images of the height and morphological features of the $CaCO_3$ precipitation layer on the surface of a biofilm. The biofilm was imaged after 15 min (left) and 4 h (right) of exposure to brine and 10 g L^{-1} urea. The height of the biofilm increased from 128 μm to 156 μm (approx.).

where they are consumed as $CaCO_3$. The solubility of bulk Ca^{2+} concentrations at various pH in brine solution was determined by Ca^{2+}-ISME and later confirmed by colorimetric assays (Table S1†).

SEM analysis of *S. pasteurii* biofilms

In addition to the chemical environment adjacent to the biofilm, the morphology of the biofilm itself was impacted by the concentration of Urea (Fig. 4). In the presence of urea, the biofilm took on a globular structural shape that increased over the 4 day growth of the biofilm. This indicates that during the initial 4 h period that the biofilm surface acted as a nucleation point for $CaCO_3$ and as time passed, the loosely precipitated $CaCO_3$ start reorganizing to form larger and more defined $CaCO_3$ crystals. The globular structure in the low urea treatment (1 g L^{-1}) remained smaller in size compared to higher urea concentration of 10 g L^{-1}.

Rate and morphology of $CaCO_3$ precipitation on biofilms

Although the formation and distinct morphological changes of $CaCO_3$ on the biofilm were observed in SEM, electron microscopy failed to provide any real time information on the evolution of the biofilm morphology as $CaCO_3$ precipitated on live bacterial cells. Hence, we used the SECM technique to map real-time morphological changes on biofilms from $CaCO_3$ precipitation (Fig. 5A and B). Fig. 5C shows representative data for the increase in biofilm height due to $CaCO_3$ precipitation from 80 to 180 μm over 4 h in the presence of 10 g L^{-1} urea and brine solution. The solid black line and solid orange line represent a negative feedback approach curve on a membrane and on a biofilm, respectively (Fig. 5C). The difference in z-direction distance determines the initial biofilm thickness. The membrane surface is considered as the reference point ($z = 0$) to calculate the initial biofilm height (solid black line in Fig. 5C). A series of approach curves were then taken on biofilm at every 30 min to determine the increase in biofilm height from $CaCO_3$ precipitation. Because the biofilm surface is heterogeneous, we monitored the biofilm height at six different locations (Fig. 5B) on the biofilm to estimate an average height for a given condition and time. Fig. 5D shows a rapid increase in average biofilm height from 95 μm to 150 μm over 4 h in the presence of the brine solution containing 10 g L^{-1} urea at 23 °C. As expected, a slower rate of increase in biofilm height or a slower $CaCO_3$ precipitation rate was observed with the brine solution containing 1 g L^{-1} urea in similar experimental conditions.

Constant-height SECM imaging was performed to assess the topology of the biofilm/precipitate layer at 15 min (Fig. 6A) and 4 h of exposure (Fig. 6B). The images show a change in morphological features of the biofilm, as shown in SEM images in Fig. 4. The overall height of the biofilm was increased from 128 μm to 156 μm over 4 h in the presence of brine solution containing 10 g L^{-1} urea.

Conclusion

Ultramicrosensors such as pH, Ca^{2+}, and redox sensors provide a powerful tool, when coupled with SECM, to monitor the local chemical process of urea hydrolysis and subsequent $CaCO_3$ precipitation by live bacterial biofilm. While high ionic strength brine solutions posed certain challenges, such as short lifetime of pH microsensors, those challenges were able to be overcome allowing application of these novel techniques to environments that are known to contain brine. Through this application we found that the chemical environment adjacent to biofilms reached a quasi-steady state within 2–10 minutes for pH and Ca^{2+} and that the impact of the biofilm extended 600 μm. The biofilm height, along with the precipitated $CaCO_3$, reached the steady state within 4 h. These findings suggest that while the bacterial enzymes played a critical role in establishing the initial chemical gradient, the slow chemical process of restructuring the $CaCO_3$ crystals was the rate-limiting step. While these measurements were performed in a petri dish, and thus boundary layer dynamics

likely played an important role the overall kinetics of the observed reactions, our data provide a new avenue for spatial and temporal measurements of pH and Ca^{2+} on scales pertain to microbial-mediated chemical processes. As a result, our data provide the insights that could be used to elucidate kinetic parameters and assist in developing an empirical model for this and other processes on biofilms. As we explore bioremediation and bioengineering approaches to mitigate todays ecological challenges, such data and approaches will be essential in optimizing environmental remediation efforts involving biofilms, including potential use for large-scale carbon capture and storage.

Disclaimer

This report was prepared as an account of work sponsored by an agency of the United States Government. Neither the United States Government nor any agency thereof, nor any of their employees, makes any warranty, express or implied, or assumes any legal liability or responsibility for the accuracy, completeness, or usefulness of any information, apparatus, product, or process disclosed, or represents that its use would not infringe privately owned rights. Reference therein to any specific commercial product, process, or service by trade name, trademark, manufacturer, or otherwise does not necessarily constitute or imply its endorsement, recommendation, or favoring by the United States Government or any agency thereof. The views and opinions of authors expressed therein do not necessarily state or reflect those of the United States Government or any agency thereof.

Acknowledgements

This work was completed as part of National Energy Technology Laboratory (NETL) research for the Department of Energy's Pacific Coast Carbon Storage Initiative.

References

1 S. M. Frailey, J. Damico and H. E. Leetaru, *Energy Procedia*, 2011, **4**, 5487–5494.
2 A. C. Mitchell, A. J. Phillips, R. Hiebert, R. Gerlach, L. H. Spangler and A. B. Cunningham, *Int. J. Greenhouse Gas Control*, 2009, **3**, 90–99.
3 Y. Fujita, F. G. Ferris, R. D. Lawson, F. S. Colwell and R. W. Smith, *Geomicrobiol. J.*, 2000, **17**, 305–318.
4 W. A. Akber Hassan and X. Jiang, *Greenhouse Gases: Sci. Technol.*, 2012, **2**, 408–418.
5 D. J. Tobler, E. Maclachlan and V. R. Phoenix, *Ecol. Eng.*, 2012, **42**, 270–278.
6 U. Gollapudi, C. Knutson, S. Bang and M. Islam, *Chemosphere*, 1995, **30**, 695–705.
7 V. Achal, A. Mukherjee and M. S. Reddy, *J. Mater. Civ. Eng.*, 2011, **23**, 730–734.
8 S. Stocks-Fischer, J. K. Galinat and S. S. Bang, *Soil Biol. Biochem.*, 1999, **31**, 1563–1571.
9 K. Van Tittelboom, N. De Belie, W. De Muynck and W. Verstraete, *Cem. Concr. Res.*, 2010, **40**, 157–166.
10 H. M. Jonkers, A. Thijssen, G. Muyzer, O. Copuroglu and E. Schlangen, *Ecol. Eng.*, 2010, **36**, 230–235.
11 D. Sarda, H. S. Choonia, D. D. Sarode and S. S. Lele, *J. Ind. Microbiol. Biotechnol.*, 2009, **36**, 1111–5.
12 C. Qian, R. Wang, L. Cheng and J. Wang, *Chin. J. Chem.*, 2010, **28**, 847–857.
13 G. D. O. Okwadha and J. Li, *Chemosphere*, 2010, **81**, 1143–8.
14 W. De Muynck, N. De Belie and W. Verstraete, *Ecol. Eng.*, 2010, **36**, 118–136.
15 J. Dick, W. De Windt, B. De Graef, H. Saveyn, P. Van der Meeren, N. De Belie and W. Verstraete, *Biodegradation*, 2006, **17**, 357–367.
16 F. G. Ferris, V. Phoenix, Y. Fujita and R. W. Smith, *Geochim. Cosmochim. Acta*, 2004, **68**, 1701–1710.
17 F. G. Ferris, R. G. Wiese and W. S. Fyfe, *Geomicrobiol. J.*, 1994, **12**, 1–13.
18 J. W. A. Foppen and J. F. Schijven, *Water Res.*, 2006, **40**, 401–26.
19 R. Faibish, M. Elimelech and Y. Cohen, *J. Colloid Interface Sci.*, 1998, **204**, 77–86.
20 Y. Zhang and R. Dawe, *Appl. Geochem.*, 1998, **13**, 177–184.
21 W. De Muynck, K. Verbeken, N. De Belie and W. Verstraete, *Ecol. Eng.*, 2010, **36**, 99–111.
22 K. L. Bachmeier, A. E. Williams, J. R. Warmington and S. S. Bang, *J. Biotechnol.*, 2002, **93**, 171–81.
23 V. Achal, A. Mukherjee, P. C. Basu and M. S. Reddy, *J. Ind. Microbiol. Biotechnol.*, 2009, **36**, 981–8.
24 T. Zhang and I. Klapper, *Int. J. Nonlinear Mech.*, 2011, **46**, 657–666.
25 T. Zhang and I. Klapper, *Water Sci. Technol.*, 2010, **61**, 2957–64.
26 S. Dupraz, M. Parmentier, B. Ménez and F. Guyot, *Chem. Geol.*, 2009, **265**, 44–53.
27 S. Amemiya, A. J. Bard, F.-R. F. Fan, M. V. Mirkin and P. R. Unwin, *Annu. Rev. Anal. Chem.*, 2008, **1**, 95–131.
28 D. Koley and A. J. Bard, *Proc. Natl. Acad. Sci. U. S. A.*, 2010, **107**, 16783–7.
29 D. Koley and A. J. Bard, *Proc. Natl. Acad. Sci. U. S. A.*, 2012, **109**, 11522–11527.
30 D. Koley, M. M. Ramsey, A. J. Bard and M. Whiteley, *Proc. Natl. Acad. Sci. U. S. A.*, 2011, **108**, 19996–20001.
31 X. Liu, M. M. Ramsey, X. Chen, D. Koley, M. Whiteley and A. J. Bard, *Proc. Natl. Acad. Sci. U. S. A.*, 2011, **108**, 2668–73.
32 J. G. Ummadi, V. S. Joshi, P. R. Gupta, A. K. Indra and D. Koley, *Anal. Methods*, 2015, **7**, 8826–8831.
33 Y. Ha, D. Myung, J. H. Shim, M. H. Kim and Y. Lee, *Analyst*, 2013, **138**, 5258–64.
34 K. Yamamoto, *Anal. Chim. Acta*, 2003, **480**, 109–117.
35 B. R. Horrocks, M. V. Mirkin, D. T. Pierce, A. J. Bard, G. Nagy and K. Toth, *Anal. Chem.*, 1993, **65**, 1213–1224.
36 X. Zhang, B. Ogorevc and J. Wang, *Anal. Chim. Acta*, 2002, **452**, 1–10.

37 M. Etienne, A. Schulte, S. Mann, G. Jordan, I. D. Dietzel and W. Schuhmann, *Anal. Chem.*, 2004, **76**, 3682–8.
38 A. C. Mitchell, A. Phillips, L. Schultz, S. Parks, L. Spangler, A. B. Cunningham and R. Gerlach, *Int. J. Greenhouse Gas Control*, 2013, **15**, 86–96.
39 C. Verba, W. O'Connor, G. Rush, J. Palandri, M. Reed and J. Ideker, *Int. J. Greenhouse Gas Control*, 2014, **23**, 119–134.
40 A. C. Mitchell, K. Dideriksen, L. H. Spangler, A. B. Cunningham and R. Gerlach, *Environ. Sci. Technol.*, 2010, **44**, 5270–6.